Turbulence: Space-time statistical properties and behavior in supersonic flows

Alexandre Favre

Citation: Physics of Fluids **26**, 2851 (1983); doi: 10.1063/1.864049
View online: http://dx.doi.org/10.1063/1.864049
View Table of Contents: http://scitation.aip.org/content/aip/journal/pof1/26/10?ver=pdfcov
Published by the AIP Publishing

Turbulence: space-time statistical properties and behavior in supersonic flows[a)]

Alexandre Favre
Institut de Mécanique Statistique de la Turbulence, Laboratoire Associé au C. N. R. S., Marseille, France

(Received 18 June 1982; accepted 7 June 1983)

Following a scientific cooperation beginning in 1954 with L. S. G. Kovasznay, and in his memory, in this paper is presented a survey of two of the main areas of research to which he contributed: (1) turbulence properties deduced through statistical conditional sampling and space-time measurements of correlations and contingencies; these include celerities, optimum correlations, memories, and coherent structures; and (2) the study of turbulence in supersonic flows initiated by Kovasznay; these include the use of mass-weighted averages, decrease of turbulence in expansion, increase in compression, strong Reynolds analogy extension, and temperature–velocity correlation conservation.

I. TURBULENCE PROPERTIES OBTAINED BY SPACE-TIME STATISTICAL METHODS

The instantaneous turbulent flow patterns are very irregular in a seemingly random manner thus suggesting that a statistical description is convenient to characterize it. Early in the development of the field, correlations were recognized as one of the more meaningful statistical parameters used in the formulation of theories and for the experimental acquisition of data. To include *temporal* variations as well as the spatial properties, the Eulerian space-time statistical relations, such as correlation coefficients of the turbulence field at different spatial locations and at different times, were introduced by Favre[1–4] with a novel experimental technique for measuring space-time correlations. He utilized a multichannel magnetic tape for a storage device for signals recorded at different spatial locations. A time delay was introduced by using two different playback heads with a variable amount of tape between them. Earlier reviews[5,6] have summarized much of this research which was developed with the cooperation of J. Gaviglio and R. Dumas[7–15] and co-workers at the Institut de Mécanique Statistique de la Turbulence.[16–32] This review emphasizes the research which was of keen interest to L. S. G. Kovasznay and points out some areas of collaboration which the I. M. S. T. had with Kovasznay dating back to 1954.

The coordinate system adopted here is shown in Fig. 1. It is assumed that the flow is stationary and has a mean velocity V in the direction x_1. The measuring stations are at P_0 and P as shown. The space-time double correlation $R_{i,j}(P_0,P,\tau)$ and the corresponding coefficient $r_{i,j}(P_0,P,\tau)$ between a velocity component $u_i'(0,0,0,t)$ at the point $P_0(0,0,0)$ at time t and the component $u_j'(X_1,X_2,X_3,t+\tau)$ at the point $P(X_1,X_2,X_3)$ at the time $t+\tau$ are

$$R_{i,j}(P_0,P,\tau) = \overline{u_i'(0,0,0,t)u_j'(X_1,X_2,X_3,t+\tau)},$$

$$r_{i,j}(P_0,P,\tau) = R_{i,j}\left[\overline{(u_i'^2)}_{P_0}\ \overline{(u_j'^2)}_{P}\right]^{-1/2}.$$

The equation for the evolution of $R_{i,j}$, written for incompressible flows,[17] inevitably introduces the space-time triple correlations and the corresponding coefficients:

$$R_{i,jk}(P_0,P,\tau) = \overline{u_i'(0,0,0,t)\{u_j'\,u_k'\}(X_1,X_2,X_3,t+\tau)},$$

$$r_{i,jk}(P_0,P,\tau) = R_{i,jk}\left[\overline{(u_i'^2)}_{P_0}\ \overline{(u_i'u_j' - \overline{u_i'u_j'})^2}_{P}\right]^{-1/2}.$$

Double and triple correlations for the two points P_0 and P are also used for the temperature θ. The three-point triple correlation at the points $P_0(0,0,0)$ at time t, and $P_1(X_1,0,|X_3|)$ and $P_2(X_1,0,-|X_3|)$ at the time $t+\tau$ is

$$R_{\theta_0,\theta_1,\theta_2}(P_0,P_1,P_2,\tau)$$

$$= \overline{\theta_0'(0,0,0,t)\{\theta_1'(X_1,0,|X_3|,t+\tau)\theta_2'(X_1,0,-|X_3|,t+\tau)\}},$$

with the corresponding correlation coefficients:

$$r_{\theta_0,\theta_1,\theta_2}(P_0,P_1,P_2,\tau)$$

$$= R_{\theta_0,\theta_1,\theta_2}\left[\overline{\theta_0'^2}\ \overline{(\theta_1'\theta_2' - \overline{\theta_1'\theta_2'})^2}\right]^{-1/2}.$$

Measurements were carried out in wind tunnels at low speeds for two flow conditions: (1) downstream of a grid in a uniform flow, $\bar{u}_1 = V$, $\bar{u}_2 = \bar{u}_3 = 0$ with constant temperature θ and mass density ρ. The turbulence was nearly isotropic and homogeneous; the Reynolds numbers based on the grid mesh M was about 21 500; (2) in boundary layers over flat plates with and without an adverse pressure gradient and with and without weak heat transfer. The Reynolds number was about 28 000 based upon the thickness δ, where

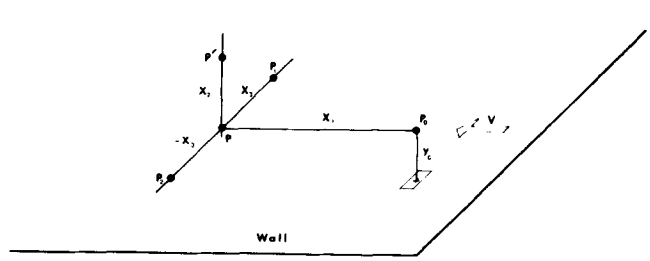

FIG. 1. Measurement locations in boundary layer conditions.

[a)] This paper was presented 22 November 1981 at a special session of the annual meeting of the Division of Fluid Dynamics of the American Physical Society in Monterey, California honoring the memory of L. S. G. Kovasznay.

 0031-9171/83/102851-13$01.90

$\bar{u}_1$ attains a value of $0.99V$. The wall distances were y (or y_0) for the point P_0 and $y + X_2$ for the other points.

A. Taylor's hypothesis verification

According to Taylor's[33] hypothesis for homogeneous isotropic turbulence of moderate intensity, the longitudinal spatial correlation coefficient $r_{1,1}(X_1,0,0,0)$ should coincide with the temporal coefficient $r_{1,1}(0,0,0,\tau)$, with $\tau = X_1\bar{u}_1^{-1}$. The coincidence of these curves[8,24,34] supported the validity of that hypothesis. The radius of curvature of the correlation at the origin has been defined as the "Taylor microscale" independent of the flow field. An attempt to prove the hypothesis for a boundary layer showed significant differences between the correlations, with agreement only at $y = 0.24\delta$.[13,14]

B. Isotropic homogeneous turbulence: Celerity, optimum correlation

The space-time correlation coefficient $r_{1,1}(X_1,0,0,\tau)$ has been measured[5,6,8,14] for the longitudinal velocity fluctuations u_1' with a longitudinal space separation X_1 (or X) in the general direction of the flow and a delay time τ. The experimental results shown in Fig. 2 disclose that for a given separation X_1, the space-time correlation coefficient reaches a maximum, at an "optimum time delay," τ_m, which defines the "optimum space-time correlation coefficient" $r_{1,1}(X_1,0,0,\tau_m)$. This coefficient retains large values for separation distances X_1 significantly greater than the distance beyond which the spatial correlation is negligible. The optimum time delay defines a "statistical celerity component" of the turbulent field, $C_{1,11}$, which is found experimentally to be practically equal to the mean velocity of the fluid:

$$C_{1,11} = X_1\tau_m^{-1} = \overline{u_1} = V. \tag{1}$$

The turbulent homogeneous isotropic field is thus convected by the uniform mean fluid flow. But this is not true for the inhomogeneous flows, where the celerities can differ from the mean velocity.[6,12,14,16,17] Following the suggestion of Kovasznay, the optimum space-time correlation can be calculated to first approximation from the spatial correlation using a turbulence diffusion expressed by a Gaussian process. Starting with the spatial correlation, the calculation shown in Fig. 2 yields good agreement between the computed and the measured values.[6,34] In addition, experiments and calculation[5,6] show that the correlation at optimum time delay is reduced by suppression of the lowest-frequency oscillations and strongly increased when the highest ones are suppressed. Thus, as might be expected, perseverance of the optimum correlation appears to be due mainly to the low-frequency components of the fluctuations.

C. Turbulence in boundary layers and various other flows

1. Velocity space-time double correlations: celerity, optimum correlation

The double correlation coefficients $r_{1,1}(X_1,X_2,X_3,\tau)$ and $r_{1,2}(X_1,X_2,X_3,\tau)$[6,30] have been measured for the velocity fluctuations u_1', u_j' with time delay τ in boundary layers.[5,6,9–31,34] With optimum time delay these are shown in Fig. 3 along with similar correlations for various flows in other laboratories.[35–41] Note that the abscissa introduced by Corrsin,[42] and Sabot and Comte-Bellot[37] for the Lagrangian correlation is used:

$$\xi = X_1\Lambda_1^{-1}(\overline{u_1'^2})^{1/2}\bar{u}_1^{-1},$$

where

$$\Lambda = \int_0^\infty r_{1,1}(X_1,0,0,0)dX_1$$

is the longitudinal integral scale. For the "optimum time delay" $\tau_{m(i,j)}$, the absolute value of these correlations attains a maximum and retains large values at great streamwise distances. This property of the "optimum" space-time correlation coefficient then has a general character as seen in the figure.

a. Celerities in boundary layers. In a more general case,[15,17,24,34] the optimum time delay $\tau_{m(i,j)}$ discussed earlier can be utilized to define the "statistical celerity" of the tur-

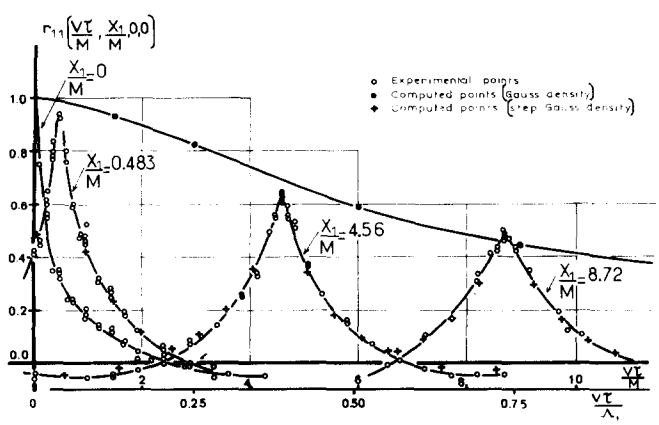

FIG. 2. Space-time double velocity correlations coefficient $r_{1,1}$, in homogeneous isotropic turbulence.

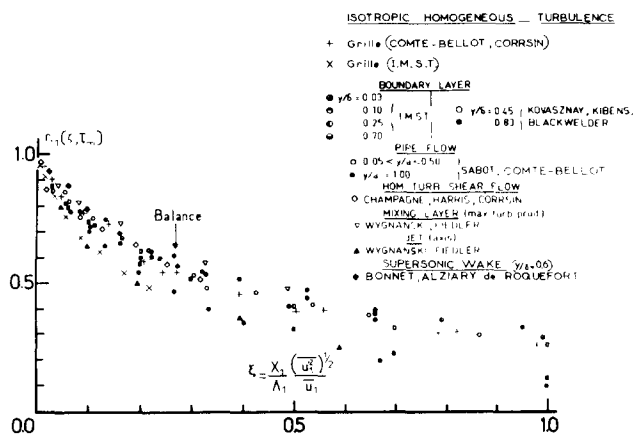

FIG. 3. Space-time double correlation coefficient $r_{1,1}$ with optimum delay in various flow fields.

bulent field. If the turbulence is band pass filtered, the celerity corresponds to a phase velocity. Several definitions of the celerity components in the direction k may be given. The following one has been chosen[17]:

$$C_{k,ij} = \left[\frac{\partial^2 R_{i,j}}{\partial \tau^2}\left(\frac{\partial^2 R_{i,j}}{\partial \tau\, \partial x_k}\right)^{-1}\right]_{\tau=\tau_{m(i,j)}}, \tag{2}$$

because it is almost independent of the separation distance. In addition, the corresponding equations can be written in simple form.[17] Furthermore, by utilizing a covariance ratio, the celerity should be independent of the magnitude of the turbulence scale. Note also that the equations retain the same formalism when the turbulent signals are filtered. These equations show that in general the celerity is different from the mean velocity of the fluid.

In homogeneous isotropic turbulence, the celerity $C_{1,11}$ in Eq. (1) reduces practically to $V = \overline{u_1}$. In the boundary layer, the celerity $C_{1,11}$ is again equal to the local mean velocity $\overline{u_1}$ for the highest-frequency fluctuations, but at lower frequencies it depends upon the location within the boundary layer; larger than $\overline{u_1}$ when $y/\delta < 0.25$ and lower when $y/\delta > 0.25$.[15,17]

b. Space-time double correlations in boundary layers. Retaining only the "optimum" values of the space-time double correlation coefficient $r_{1,1}\,(X_1,X_2,X_3,\tau_{m(1,1)})$ with the optimum delay $\tau_{m(1,1)}$, the curves of iso-space-time optimum correlation coefficients of the turbulence have been measured.[5,6,10–14,24,34] For example, in Fig. 4, it is seen for a nominally two-dimensional boundary layer with the fixed probe at $y/\delta = 0.03$, the correlation surfaces are elongated in the streamwise direction X_1, symmetric in the spanwise direction, and flattened in the orthogonal direction X_2 near the wall. The line of maximum maximorum correlation[14,34] is slightly convex towards the wall for $y/\delta = 0.03$ and concave in the outer region. For a given streamwise separation X_1, the optimum correlation decreases with the distance y to the wall.[5,6]

c. Optimum space-time correlations and flow memory. The comparison was given in Fig. 3, of the space-time double correlation coefficient $r_{1,1}\,(\xi,\tau_{m(1,1)})$ with optimum delay $\tau_{m(1,1)}$ along the mean streamlines for several flow fields,[5,6,9,10–31,35–41] homogeneous isotropic turbulence, boundary layer, pipe flow, homogeneous shear flow, mixing layer, and a wake behind a flat plate in a supersonic flow at Mach 2. The double correlation coefficients, $r_{1,1}\,(\xi,\tau_{m(1,1)})$, for these various flows agree quite well considering the diversity of flow fields included. For the shear flows, it is noteworthy that after accounting for the integral scale, Λ_1, and the intensity of turbulence, the optimum space-time correlation seems to have larger values when the production is larger than the diffusion.

This suggests the idea of statistical "memories" at the downstream point P defined now as follows:

(1) For each component of the velocity fluctuations $u_i'(P_0,t)$ and $u_i'(P,\tau_{m(i,i)})$:

$$0 \leqslant M_{u_i',u_i'}\{P_0,P,\tau_{m(i,i)}\} \equiv |r_{i,i}\{P_0,P,\tau_{m(i,i)}\}| \leqslant 1$$

(no summation over the indices, i). The present measurements are for $i = 1$;

(2) For the velocity fluctuations vectors $\mathbf{u}'(P_0,t)$ and $\mathbf{u}'(P,t+\tau)$:

$$0 \leqslant M_{\mathbf{u}'\cdot\mathbf{u}'}\{P_0,P,\tau_{m(\mathbf{u}')}\} \equiv |r_{\mathbf{u}'\cdot\mathbf{u}'}\{P_0,P,\tau_{m(\mathbf{u}')}\}| \leqslant 1,$$

$$M_{\mathbf{u}'\cdot\mathbf{u}'} \equiv |\,\overline{\mathbf{u}'(P_0,t)\cdot\mathbf{u}'\{P,t+\tau_{m(\mathbf{u}')}\}}\,| \left[\,\overline{(\mathbf{u}')^2_{P_0}}\;\overline{(\mathbf{u}')^2_{P}}\,\right]^{-1/2},$$

$$M_{\mathbf{u}\cdot\mathbf{u}'} = \{(\overline{u_i'\,u_i'})_{P_0}(\overline{u_i'\,u_i'})_P\}^{-1/2}\delta_{ij}(\overline{u_{iP_0}'^2}\;\overline{u_{jP}'^2})^{1/2} \times |r_{i,j}\{P_0,P,\tau_{m(\mathbf{u}')}\}|,$$

which has more physical meaning by introducing the space-

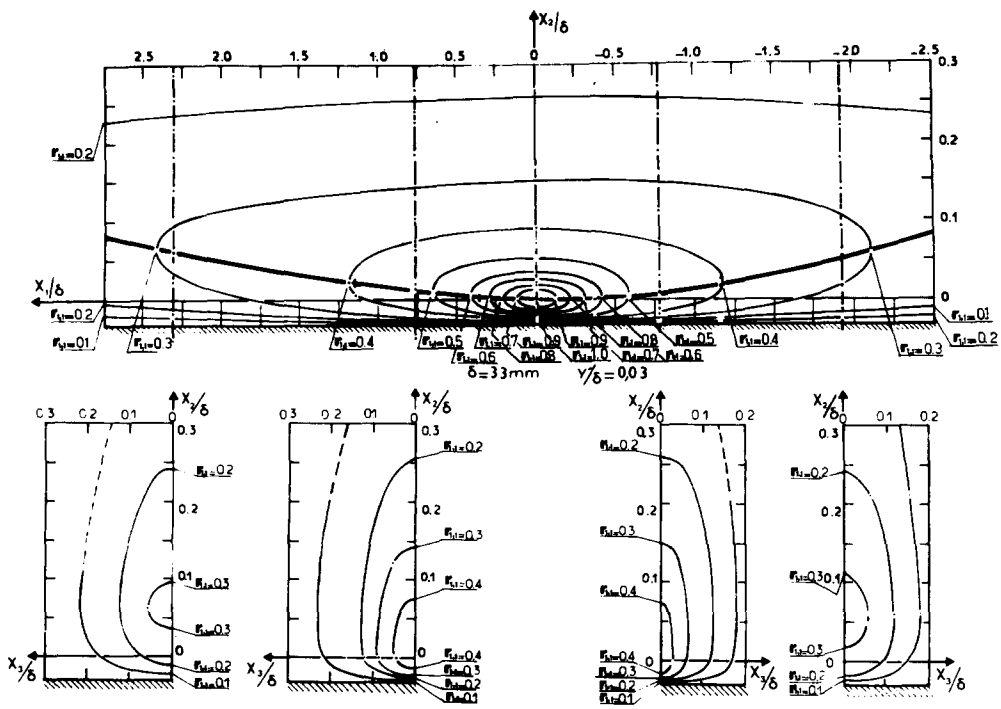

FIG. 4. Curves of constant double space-time correlation coefficient of the longitudinal velocity component with optimum delay in a boundary layer on a flat plate with $y = 0.3\delta$ and $R_\delta = 27900$.

time scalar product of the velocity fluctuations vectors[43] and which has a unique optimum time delay $\tau_{m(u')}$;

(3) For the temperature fluctuations, the statistical memory is defined in a similar fashion by

$$0 \leqslant M_{\theta'_0,\theta'}\{P_0,P,\tau_{m(\theta')}\} = |r_{\theta'_0,\theta'}\{P_0,P,\tau_{m(\theta')}\}| \leqslant 1.$$

For the case of weak heat transfer, $M_{\theta'_0,\theta'}$ has been measured primarily for the large-scale fluctuations.

These "memories" equal unity when P_0 coincides with P and $\tau_m = 0$.

2. Equations for the space-time optimum correlation

The equations for the space-time optimum correlations have been derived.[17] In a two-dimensional flow field with a mean velocity in the direction X_1, the equation for $R_{1,1}(X_1,0,0,\tau_{m(1,1)})$ was found by Dumas *et al.*[22,23] to be

$$\left[\underset{(T)}{\frac{\partial R_{1,1}}{\partial \tau}} + \underset{(T_1)}{\bar{u}_1 \frac{\partial R_{1,1}}{\partial X_1}} + \underset{(T_2)}{\bar{u} \frac{\partial R_{1,1}}{\partial X_2}} + \underset{(P_1)}{R_{1,1} \frac{\partial \bar{u}_1}{\partial X_1}} + \underset{(P_2)}{R_{1,2} \frac{\partial \bar{u}_1}{\partial X_2}} + \underset{(D_1)}{\frac{\partial R_{1,11}}{\partial X_1}} + \underset{(D_2)}{\frac{\partial R_{1,12}}{\partial X_2}} + \underset{(D_3)}{\frac{\partial R_{1,13}}{\partial X_3}} + \underset{(\pi_1)}{\frac{1}{\rho}\frac{\partial \pi_1}{\partial X_1}} - \underset{(\Delta)}{\nu\left(\frac{\partial^2 R_{1,1}}{\partial X^2_1} + \frac{\partial^2 R_{1,1}}{\partial X^2_2} + \frac{\partial^2 R_{1,1}}{\partial X^2_3}\right)}\right]_{\tau = \tau_{m(1,1)}} = 0, \tag{3}$$

where π_1 is the velocity pressure correlation:

$$\pi_1(P_0,P,\tau) = \overline{u'_1(0,0,0,t)p'(X_1,X_2,X_3,t+\tau)}. \tag{4}$$

The convection, production, turbulent diffusion, and viscous diffusion are denoted by T_i, P_i, D_i, and Δ under each respective term.

Experiments[22,23,25] have been made in the inner part $y_0/\delta = 0.056$ of a boundary layer, where the production is strong, and with a large separation $X_1 = 1.43\delta$ (see Fig. 3; $\xi \sim 0.28$) such that the low-frequency fluctuations effects are dominant and the dissipation effects associated with higher frequencies are weak. The correlation $R_{1,1}$ variation is practically equivalent to that of the correlation coefficient $r_{1,1}$ because the intensity of turbulence is nearly constant along the mean streamlines which coincide practically with $X_2 \sim X_3 \sim 0$. Under these conditions, the correlation coefficients also represent the variation of the "memory," $M_{u'_1,u'_1}$, for the fluctuations u'_1. The term π_1 has not been measured, but computed through Eq. (3), thus it contains also the errors of measurement of the other terms.

For the case of homogeneous isotropic turbulence (Sec. IB) where $T \equiv 0 = T_1 = P_1 = P_2 = \pi_1 + \pi_2 + \pi_3$ the rate of loss of the optimum correlation along the distance X_1 downstream has been explained to a first approximation neglecting the viscous effects by turbulent Gaussian diffusion (Fig. 2). In the present case of an inhomogeneous flow, the experimental values, made nondimensional (*) by $\Lambda_1(\overline{u'^2_1})^{-3/2}$, are summarized by

$$\frac{\Lambda_1}{(\overline{u'^2_1})^{3/2}_{P_0}}\Big(\underset{-1.15}{\text{convection}} + \underset{-0.85}{\text{production}} + \underset{+0.95}{\text{turbulent diffusion}} + \underset{+1.02}{\text{pressure-velocity}} + \underset{+0.03}{\text{viscosity}}\Big)_{\tau=\tau_m} = 0.$$

The rate of change of the optimum correlation $R_{1,1}(X_1,0,0,\tau_{m(1,1)})$ with $\tau = \tau_{m(1,1)}$ is: $T^* = 0$, because for $\tau = \tau_{m(1,1)}$, $\delta R_{1,1}/\delta\tau \equiv 0$ by definition, $T^*_1 = -1.15$, $T^*_2 = 0$ along the distance X_1 downstream, $P^*_1 = 0$, $P^*_2 = -0.85$ corresponding to "production," $D^*_1 = 0.34$, $D^*_2 = +0.61$ $D^*_3 = 0$ corresponding to "diffusion," $\pi^*_1 = 1.02$ corresponding to the velocity–pressure correlation, $-\Delta^* = 0.03$ corresponding to viscosity effects. Thus, at this position in the boundary layer, the loss of correlation along the distance X_1 downstream is explained by the turbulent diffusion, but in addition there are losses by velocity–pressure correlation and by viscosity effects. There is a "production" term of the space-time optimum correlation $R_{1,1}(X_1,0,0,\tau_{m(1,1)})$ (playing a role analogous to the production of turbulence) which contributes to maintain the corresponding optimum correlation and "memory." This can be understood by the fact that these terms of "production" of $R_{i,j}(P_0,P,\tau_{m(i,j)})$ are proportional to the space-time optimum correlation $R_{k,j}(P_0,P,\tau_{m(i,j)})$ of the upstream turbulence, times the mean velocity derivatives $\partial\bar{u}_i/\partial x_k$. In this gradient-type flow, these are of the same sign thus yielding positive production of the correlation.

3. Velocity or temperature space-time double and triple correlations and conditional correlations: Structures of turbulence in a boundary layer

The space-time double and triple correlations, compared with spatial correlations, can be used to investigate the structures of the turbulent fields. Experiments have been made in a boundary layer with large separation distances so the correlations are due primarily to the large structures.

a. Velocity double and triple space-time correlations. The measurements of double and triple space-time correlations[18,19,30] between a velocity component at point P_0 and time t and one or two components of fluctuations at point $P'(X_1,X_2,0)$ at time $t+\tau$ gives the signs of the fluctuations and provides additional information about the turbulent "eddies." For example, in the wall region, low-momentum fluid moving away from the wall, $u'_1 < 0$; $u'_2 > 0$, corresponds to "ejected eddies" or "bursts." On the other hand, higher momentum fluid moving toward the wall, $u'_1 > 0$; $u'_2 < 0$, corresponds to "sweeps" as described by the visualizations of Kline *et al.*[44]

b. Temperature double and triple space-time correlations. To obtain more information on the description of these structures, the wall of the plate was slightly heated so the heat marked the fluid as a passive contaminant. The description of a scalar is simpler than that of the velocity and in addition, the sign of the temperature fluctuation indicates the origin of the fluid lumps.[20,21,23,25,26,28,30,31]

To determine the spanwise dimension of the large scale structures, Kovasznay suggested the measurement of temperature fluctuations θ' not only at two points, but also at

three points as indicated in Fig. 1. The triple space-time correlation coefficient $r_{\theta_0,\theta_1,\theta_2}$ (P_0,P_1,P_2,τ) could be calculated from data obtained at point P_0 at time t and at the two symmetric points $P_1(X_1,0,|X_3|)$ and $P_2(X_1,0,-|X_3|)$ at the same time $t+\tau$. If the triple correlation has a fairly high value at $\tau=\tau_{m(\theta)}$, the physical interpretation may be that a disturbance passing through P_0 at time t reaches the symmetric points P_1 and P_2 simultaneously at the time $t+\tau_{m(\theta)}$. This means statistically that the spanwise length of coherence of these structures is at least of the order of the distance P_1P_2. In contrast, the double correlation cannot distinguish between a small perturbation which has a very sinuous path and a large less active one, and consequently, it can yield only the spanwise length of influence.

Figure 5 shows the comparison between the double and triple space-time isocorrelation coefficients measured in the inner boundary layer at $y/\delta=0.034$ as functions of the time delay τ and the spanwise symmetrical separations X_3. They can be compared also with the classic space correlations as discussed below. For the double isocorrelations, the dotted line enclosed the area of positive values, which may be called the "zone of influence." It has a streamwise length of several δ and a spanwise length of about 0.5δ. For the triple isocorrelations, the dotted lines encloses the area of positive values, which may be called the "zone of coherence." It gives an idea of the span of the large scale structures, which is much narrower.

An interpretation of these results is given in Fig. 6, showing the zero lines of the double space-time correlation coefficient r_{θ_0,θ_1} (P_0,P_1,τ), the triple space-time correlation coefficient $r_{\theta_0,\theta_1,\theta_2}$ (P_0,P_1,P_2,τ), and the spatial spanwise correlation coefficient r_{θ_1,θ_2} $(P_1,P_2,\tau=0)$. These lines define a mapping of the space, according to the signs of these various correlations. Three modes are statistically dominant and correspond to

I. $r_{\theta_0,\theta_1,\theta_2}>0$; $r_{\theta_0,\theta_1}>0$; $r_{\theta_0,\theta_2}>0$; $r_{\theta_1,\theta_2}>0$; $\theta_0'>0$; $\theta_1'>0$; $\theta_2'>0$,

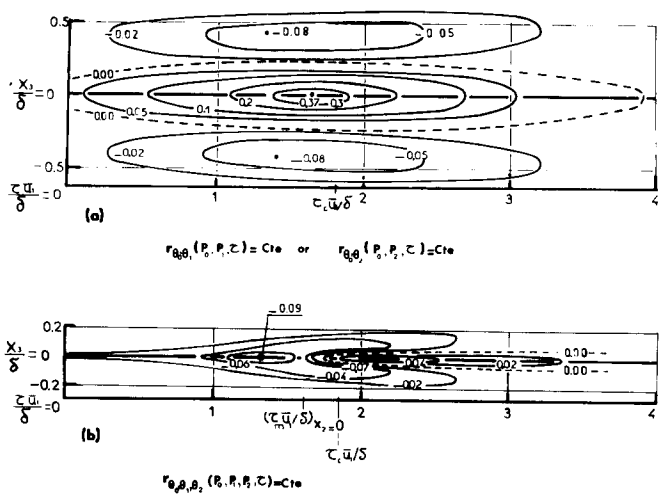

FIG. 5. Isocoefficients of double (a) and triple (b) space-time temperature correlations in a boundary layer at three points: upstream at $P_0=(0,0,0)$ and downstream at $P_1(X_1=1.86\delta,\ X_2=0,\ |X_3|,\tau)$ and $P_2(X_1=1.86\delta,\ X_2=0,\ -|X_3|,\tau)$.

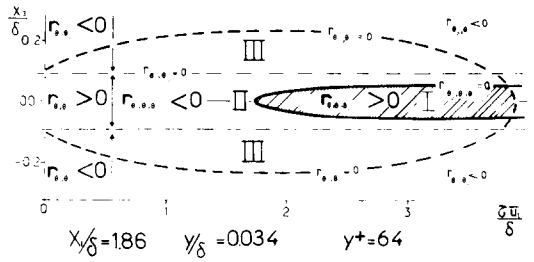

FIG. 6. Interpretation of the two- and three-point double and triple space-time correlations in a boundary layer at $X_1/\delta=1.86$ and $y/\delta=0.034$ $(y^+=64)$.

hot fluid, originating from the region nearer the wall, passing through P_0 transported downstream and appearing simultaneously at P_1 and P_2. This type of motion corresponds to the "bursts."

II. $r_{\theta_0,\theta_1,\theta_2}<0$; $r_{\theta_0,\theta_1}>0$; $r_{\theta_0,\theta_2}>0$; $r_{\theta_1,\theta_2}>0$; $\theta_0'<0$; $\theta_1'<0$; $\theta_2'<0$,

cold fluid from a region further from the wall, passing through P_0, transported downstream and appearing simultaneously at P_1 and P_2 which corresponds to the "sweeps."

III. $r_{\theta_0,\theta_1,\theta_2}<0$; $r_{\theta_0,\theta_1}>0$; $r_{\theta_0,\theta_2}>0$; $r_{\theta_1,\theta_2}<0$; $\theta_0'>0$; $\theta_1'\theta_2'<0$,

hot fluid passing through P_0 and traveling obliquely only to P_1 or to P_2, correlated with cold fluid passing over P_1 or P_2, to satisfy the mass budget.

Figure 7 sums up the results on modes for three typical distances from the wall; in the inner region $y/\delta=0.034$, in the central region $y/\delta=0.34$ and in the intermittent region, $y/\delta=0.82$ $(\gamma=0.45)$. Focusing on the hatched zone I, corresponding to the hot fluid coming from the region nearer the wall, one sees that the correlated span of the large scale structure, i.e., "ejected eddies" or "bursts" increases across the boundary layer, from 0.1δ in the inner part to 0.8δ in the intermittent part. The three-dimensional nature of the large-scale structure is therefore exemplified.

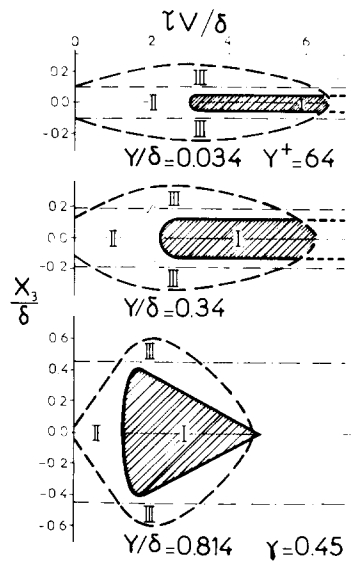

FIG. 7. Dominant correlation patterns in a boundary layer illustrating the turbulent structures.

In the intermittent region, the discrimination between turbulent and nonturbulent flow is better obtained by using temperature signals because they are not disturbed by the irrotational velocity fluctuations. Figure 8 gives a comparison[21,26] between the space-time double correlations maps for temperature and for the intermittency function measured by Kovasznay *et al.*[36] which agree and show that the temperature can be used as indicator for turbulent zones.

c. Temperature conditioned space-time correlations. In order to improve the interpretation of the previous results, measurements have been made[21,23,25,26,30,31] of space-time two-point correlations conditioned by the sign of the temperature fluctuations with an indicator function $J(t) = 1$ or zero obtained at the two points P_0 and P as explained below. The definitions of the two-point conditional space-time double and triple correlations $R_{m,n}(\tau)$ and $R_{m,nn}(\tau)$, which are not correlation coefficients $r_{\theta_0,\theta}$ and r_{θ_0,θ^2} are

$$R_{m,n(\tau)} = \overline{J(t)\theta'_0(t)_{P_0}\theta'(t+\tau)_P}\left(\overline{\theta'^2_0}\;\overline{\theta'^2}\right)^{-1/2},$$

$$R_{m,nn(\tau)} = \overline{J(t)\theta'_0(t)_{P_0}\theta'^2(t+\tau)_P} \times\left[\overline{\theta'^2_0}\;\overline{(\theta'^2-\theta'^2)^2}\right]^{-1/2},$$

where m and n are the signs $+$ or $-$. $J(t) = 1$ if $\theta'_0(t)_{P_0}$ and $\theta'(r+\tau)_P$ have the signs designated by m and n; otherwise $J(t) = 0$. The total coefficients of the space time correlations are

$$r_{\theta_0,\theta} = R_{++} + R_{+-} + R_{-+} + R_{--},$$

$$r_{\theta_0,\theta^2} = R_{+++} + R_{+--} + R_{-++} + R_{+++}.$$

Figure 9 gives the double correlation coefficient $r_{\theta_0,\theta}$ denoted by r and the conditional correlations $R_{m,n}$ for two points on the same streamline in the intermittent region of the boundary layer where τ^* is $\tau V/\delta$. Here τ_c^* is the time corresponding to the local mean velocity $\tau_c^* = (X_1\cdot\delta^{-1}) \times (V\cdot\bar{u}_1{}^{-1})$ and γ the intermittency. The coefficient r reaches a maximum value for an optimum time delay $\tau_{m(\theta)}$ which in this region is practically the same for all the conditional correlations $R_{++}, R_{--}, R_{+-}, R_{-+}$. For asymptotic time delays, the conditional correlations tend to the Gaussian values for independent variables: $\pm(2\pi)^{-1}$. Near the time $\tau_{m(\theta)}$ the correlations R_{+-} and R_{-+} are almost nil and the main contributions are from R_{++} and R_{--}.

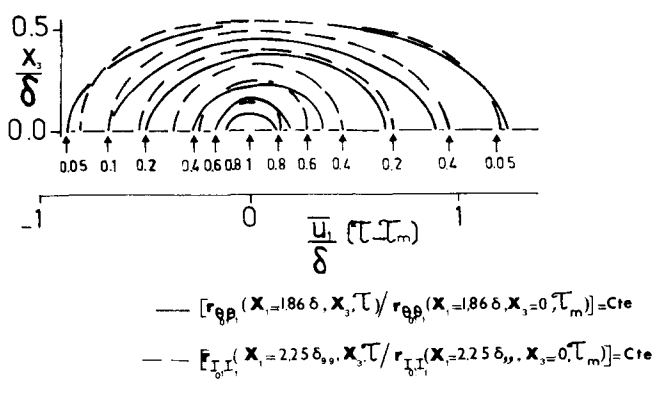

FIG. 8. Comparison between the space-time correlation of temperature and the intermittency function I introduced by Kovasznay.

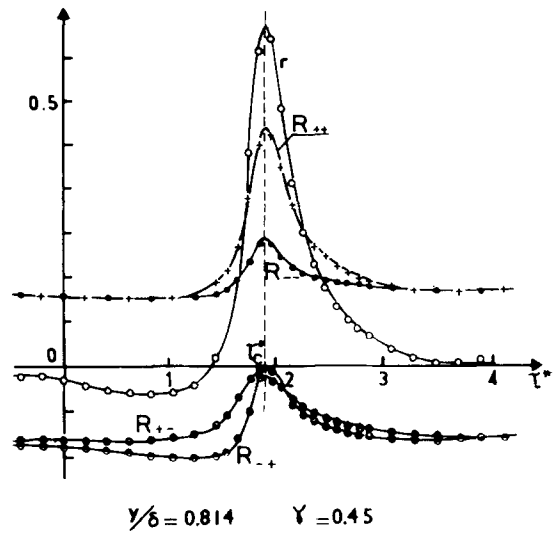

FIG. 9. Double conditional space-time correlations in the intermittent region of boundary layer at $y/\delta = 0.81$ and $\gamma = 0.45$.

Figure 10 shows similar results on a mean streamline for double and triple conditional correlations in the central zone $y/\delta = 0.34$ where there is no intermittency. In Fig. 10(a) the optimum delay for R_{++} is higher that for R_{--}; thus the celerity of coherent hot lumps coming from the wall is lower than that of the cold fluid lumps coming from the external side agreeing with the velocity correlation (Sec. IC1a). When the distance from the wall decreases, this effect increases. In addition, the optimum delay for R_{++} becomes

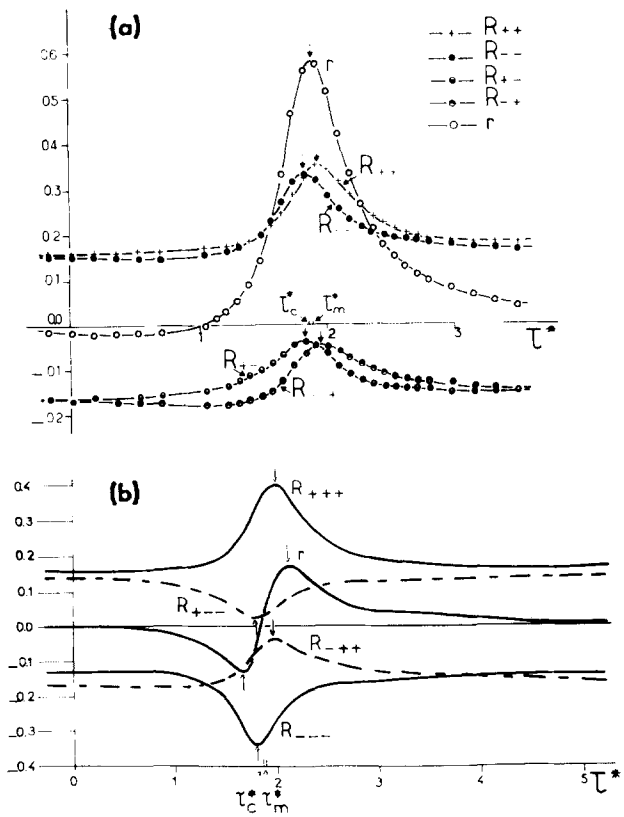

FIG. 10. Conditional space-time double (a) and triple (b) correlations in the central zone of boundary layer: $y = 0.3398\delta$, $\gamma \cong 1$, $X_1 = 1.86\delta$.

smaller than τ_c in the inner region indicating there are highly correlated lumps, coming from the wall region, which travel faster than the mean local velocity $\bar{u}_1$.

In Fig. 10(b) the triple coefficient of the conditional correlations is given. As usual in fully turbulent zones, the triple total correlation coefficient has relatively low values. It has been separated into conditional correlations of opposite signs and it has an antisymmetrical pattern since the celerities of hot and cold lumps are different, and the extremums do not occur for the same optimum time delays. These results confirm that the dominant modes are those in which the upstream hot fluid remains hot downstream and similarly for the cold fluid. Thus the structures are relatively well conserved along the mean streamlines.

4. Conditional space-time probabilities and contingencies

Turbulence is principally generated in the buffer layer by the bursting process. A study of this structure has been carried out using temperature measurements by locating the upstream point P_0 near the wall at $y_0/\delta = 0.013$, while the downstream point P' at $X_1/\delta = 0.93$ was moved in a direction orthogonal to the wall. This experimental condition contrasts that utilized in the correlation studies where the two points were located on the mean streamline.

In order to determine the statistical relationship, the conditional space-time probabilities and the corresponding contingency have been defined.[25,27,31] The temperature fluctuations θ'_0 and θ', normalized by their standard deviations, σ_0 and σ, were utilized to define the following: the probability that $\theta'_0/\sigma_0 > h_0$, the probability that $\theta'/\sigma > h$, the joint probability that $\theta'_0/\sigma_0 > h_0$ and $\theta'/\sigma > h$, and the conditional probability that $\theta'/\sigma > h$ if $\theta'_0/\sigma_0 > h_0$, where h_0 and h are the thresholds. This allows a space-time contingency ϕ and a corresponding reduced contingency Φ to be defined for hot fluid as

$$\phi \equiv \text{Prob}\left(\frac{\theta'_0(t)}{\sigma_0} > h_0 \text{ and } \frac{\theta'(t+\tau)}{\sigma} > h\right) - \text{Prob}\left(\frac{\theta'_0(t)}{\sigma_0} > h_0\right) \text{Prob}\left(\frac{\theta'(t+\tau)}{\sigma} > h\right),$$

$$\Phi \equiv \phi \left[\text{Prob}\left(\frac{\theta'_0(t)}{\sigma_0} > h_0\right)\left(1 - \text{Prob}\,\frac{\theta'(t+\tau)}{\sigma} > h\right)\right]^{-1},$$

$$\Phi = \left[\text{Prob}\left(\frac{\theta'(t+\tau)}{\sigma} > h \text{ if } \frac{\theta'_0(t)}{\sigma_0} > h_0\right) - \text{Prob}\left(\frac{\theta'(t+\tau)}{\sigma} > h\right)\right] \times \left(1 - \text{Prob}\,\frac{\theta'(t+\tau)}{\sigma} > h\right)^{-1}.$$

The usual definitions from probability theory imply that complete independence between θ_0 and θ is found if $\Phi = 0$ and total dependence yields $\Phi = 1$. For brevity, Φ^{++} is used to denote the reduced contingency for the possible temperature excursions, $\theta'_0 > 0$ and $\theta' > 0$. Conversely for the negative excursions associated with the cold fluid, $\theta'_0 < 0$ and $\theta' < 0$, symmetrical definitions are used with $\theta'_0/\sigma_0 < -h_0$ and $\theta'/\sigma < -h$. Similarly, the reduced contingency Φ^{--} is used.

For different threshold levels, Figs. 11(a)–11(c) present the reduced contingencies Φ^{++} for hot and Φ^{--} for cold fluid as functions of the distance from the wall with the longitudinal separation being fixed. The time delay has the optimum value for the correlation coefficient in section X_1. It is practically the same for the maximum maximorum values of Φ^{++} or Φ^{--}, with $h_0 = h = 0$. It appears that as the threshold become larger, the contingencies are increasingly different from the Gaussian values. Figure 11(d) shows the conditional correlations R_{++} and R_{--}. After subtracting the limiting value of $(2\pi)^{-1}$ for independent variables, they look like the contingencies Φ^{++} and Φ^{--} for $h_0 = h = 1$ or 1.5. One can infer that second-order correlations are significant principally for the perturbations containing relatively important turbulent energy.

With the aim of obtaining a picture of the diffusion, Fig. 12 gives a Lagrangian representation of the contingencies Φ^{++} with $h_0 = h = 1$, corresponding to the marked hot-fluid lumps coming from the wall region. The lines correspond to constant values of the contingencies equal to one half of the maximum maximorum value of Φ^{++} at the same optimum delay τ^*. In addition, the dashed line represents the maximum maximorum contingency, which has a slope of 2.4%, in excellent agreement with Shlien and Corrsin[45] who have found a slope of 2.5% for the line of maximum concentration for diffusion from a real source. However, one cannot consider the upstream point P_0 as a source point since

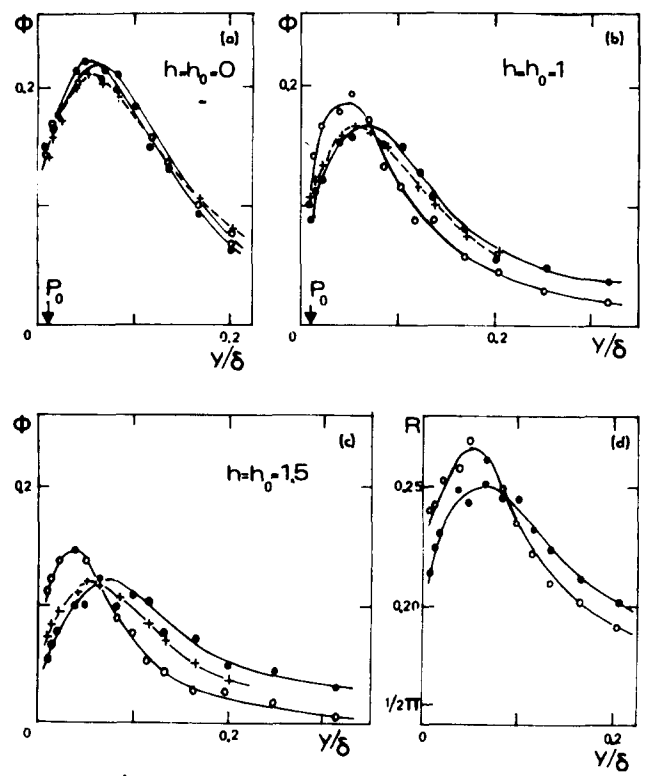

FIG. 11. Reduced contingencies Φ^{++} for hot and Φ^{--} for cold fluid with thresholds of zero (a); 1.0 (b); and 1.5 (c). The conditional space-time correlations are shown in (d).

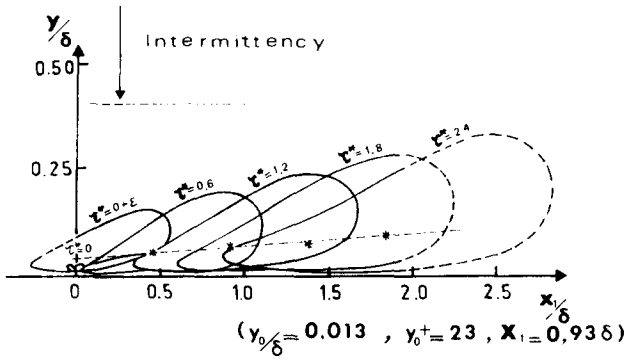

FIG. 12. Relative isocontingencies of hot fluid lumps for $y_0 = 0.013\delta$ ($y^+ = 23$) and $X_1 = 0.93\delta$. The curves represent $\Phi^{++}/\Phi^{++}_{max} = 0.5$ at the indicated time delays with both thresholds equal to unity. The positions of $\Phi^{++}/\Phi_{max} = 1$ are denoted by the *.

the correlated particles passing through the downstream point can come from the neighborhood of P_0 where the temperature fluctuations are strongly correlated with that at P_0. Thus, an initial source region for time $\tau^* = 0 + \epsilon$ has been drawn by taking half the virtual maximum value obtained as τ^* tended to zero which is 0.22.[31]

It appears in Fig. 12 that the initial contour of the source region has the same shape as the others and they enlarge regularly with time. This result is in agreement with the self-similarity proposed by Batchelor for the Lagrangian dispersion[34] in the constant stress layer.

Thus the main feature concerns the celerity of the hot fluid associated with ejected eddies or bursts and which appears to be higher than the mean velocity in the inner region. This confirms that during the bursting process inrushes of high velocity fluid interact with low velocity streaks ejected from the wall region and carry them across the boundary layer, in agreement with the most favored trajectory of "ejected eddies" visualized by Kline *et al.*[44]

D. CONCLUSION

The concepts of space-time correlations, higher moments, probabilities, and conditional sampling, the latter developed in collaboration with Kovasznay, have been applied successfully to several turbulent flows, including a concentrated study of boundary layers. These techniques give the celerities of the entire field, or of the selected constituents of the field, and permits one to follow the field with the corresponding celerity. These methods also allow the measurement of the optimum correlation coefficient and help elucidate the various competing mechanisms involved; namely loss by diffusion, by pressure–velocity correlations, and by viscosity, and gain through the production. These techniques help describe the turbulent eddy structures, such as the "bursts" and "sweep" and their interaction, and permit an indirect approach to the diffusion mechanism.

The experiments have been performed in several classical flow fields, such as homogeneous isotropic turbulence, boundary layers, pipe flows, homogeneous shear flows, mixing layers, the wakes of supersonic flat plates, etc. It would be useful to complete these investigations and to extend them to more complex cases, such as three-dimensional boundary layers, counter-gradient flows, mixing of turbulent flows of different characteristics, stratified flows, and the supersonic expansion and shock wave that we shall consider in Sec. II.

It would be useful, especially for complex flows, to introduce the space-time statistical information into the equations to help with closure. As suggested by Kovasznay and Favre,[29] the volume-dependent terms such as pressure, vorticity, and large conservative structures could be modeled in the streamwise elongated zones where the space-time optimum correlations are significant, taking into account the "history" of the turbulence.

II. TURBULENCE IN SOME SUPERSONIC FLOWS

Since 1950–1953, Kovasznay[46] was the main initiator of the investigations of turbulence in supersonic flows. He pioneered the decomposition of compressible turbulence into its "three modes" and showed how to determine their levels and correlations from measurements of mass flow and stagnation temperature fluctuations performed by the hot-wire anemometer with interpretation by his diagram method. With his cooperation, this research was extended at the I. M. S. T. into areas of turbulent heat transfer[17,24] and later to turbulence in supersonic flows with J. Gaviglio and coworkers.[24,47–53] A supersonic wind tunnel was especially built for that purpose in 1961. According to Morkovin's hypothesis[24] for supersonic flows in quasiequilibrium, the turbulent field is not very different from that of incompressible flows with heat sources. Therefore, some supersonic stationary flows that were strongly out of equilibrium were investigated to focus on more specific effects of density variations.

A. Analytical considerations

For the fluid flows with variable density, Favre[24,54–59] has developed statistical equations using the mass-weighted average method. A transportable quantity w is separated into a mass-averaged part $\tilde{w}$ and a fluctuation w' such that

$$w \equiv \tilde{w} + w' \text{ with } \bar{\rho}\tilde{w} \equiv \overline{\rho w} \Leftrightarrow \overline{\rho w'} \equiv 0 \Leftrightarrow \overline{w'} \equiv -\overline{\rho' w'}/\bar{\rho}, \tag{5}$$

and as usual,

$$\rho \equiv \bar{\rho} + \rho' = \Leftrightarrow \bar{\rho}' \equiv 0.$$

In this case the mass conservation equation simplifies to

$$\frac{D\bar{\rho}}{Dt} \equiv \frac{\partial \bar{\rho}}{\partial t} + \tilde{u}_k \frac{\partial \bar{\rho}}{\partial x_k} = -\bar{\rho}\frac{\partial \tilde{u}_i}{\partial x_i}. \tag{6}$$

Thus, the mean value of the kinetic turbulent energy is $\frac{1}{2}\overline{\rho u_i' u_i'}$ and its production is expressed by

$$P = -\overline{\rho u_k' u_1'}\frac{\partial \tilde{u}_i}{\partial x_k} - \overline{u_i' \frac{\partial p}{\partial x_i}}. \tag{7}$$

The first term on the right-hand side may be called the "kinetic production" P_c and the other term the "enthalpic production" P_e, because they describe exchanges, respectively, of the kinetic and enthalpic energy.

The kinetic production may be written[24,57,58]

$$P_c = -\frac{1}{3}\,\overline{\rho u_j' u_j'}\,\frac{\partial \tilde{u}_i}{\partial x_i} - \left(\overline{\rho u_k' u_i'} - \frac{1}{3}\,\overline{\rho u_j' u_j'}\,\delta_{ik}\right)\frac{1}{2}\left(\frac{\partial \tilde{u}_i}{\partial x_k} + \frac{\partial \tilde{u}_k}{\partial x_i}\right), \quad (8)$$

since the term including the mean rotation tensor is null. Splitting the symmetric rate of strain tensor into a dilation rate and an isovolumetric part and using mass conservation, Eq. (6), P_c may also be written as[48,49]

$$P_c = \frac{1}{3}\,\overline{\rho u_j' u_j'}\,\frac{1}{\bar{\rho}}\,\frac{D\bar{\rho}}{Dt} - \left(\overline{\rho u_k' u_i'} - \frac{1}{3}\,\overline{\rho u_j' u_j'}\,\delta_{ik}\right) \times\left[\frac{1}{2}\left(\frac{\partial \tilde{u}_i}{\partial x_k} + \frac{\partial \bar{u}_k}{\partial x_i}\right) + \frac{1}{3}\,\frac{1}{\bar{\rho}}\,\frac{D\bar{\rho}}{Dt}\,\delta_{ik}\right], \quad (9)$$

and all the other terms are null. The first term on the right-hand side is the isotropic part of the Reynolds stress tensor, multiplied by the rate of the mean mass-weighted density variation; it is negative in expansion and positive in compression. The second term expresses the interaction between the anisotropic part of the Reynolds stress tensor and the isovolumetric part of the strain rate.

The enthalpic production may be written[24]

$$P_e = -\frac{\partial}{\partial x_i}\left(\overline{u_i' p'}\right) + p'\,\frac{\partial u_i'}{\partial x_i} + \frac{\overline{\rho' u_i'}}{\bar{\rho}}\,\frac{\partial \bar{p}}{\partial x_i}. \quad (10)$$

The first term on the right-hand side is usually analyzed together with the diffusion terms. The second one is usually considered as small for flows at moderate Mach numbers. The last term may be important when the density fluctuations are correlated with the velocity and when the mean pressure gradient is strong. When the pressure gradient is due to the gravity, it produces buoyancy. Correspondingly when it is due to the inertia, for instance in supersonic flows, it produces analogous effects. The sign of the density–velocity correlation and the mean pressure gradient determine whether that term of enthalpic mean production will be positive or negative.

This simple analysis explains the mechanism of production of turbulence with the effects of the mean density variation and of the density fluctuations. For instance in the three following types of flow, the turbulence decreases in expansion and increases in compression.

B. Axisymmetric near-wake in a supersonic flow

The model chosen was a cylinder parallel to the mean flow[47–50] at Mach number 2.3. The initial boundary layer was fully turbulent and the Reynolds number based on the momentum thickness was 10^3. The boundary layer separated from the base wedge along a recirculation zone, was accelerated by an expansion fan, formed a mixing layer which was subjected to a compression by turning at the neck of the near-wake with a shock wave, and then transformed to a self-preserving far-wake.

Figure 13 shows the mean "stream lines" which are tangent to the mean mass-weighted velocity.[50] It shows also the mean pressure $\bar{p}$ in the mixing layer, where $p(0)$ is the pressure in the external upstream flow. The pressure gradient, strongly negative in the separation zone, becomes null, and then positive in the shock wave zone. The total shear stress[47,49,50] increased in the mixing layer and reaches a maximum in the zone where the pressure gradient is maximum, which is several times greater than the initial value at the wall, and then decreases downstream.

Figure 14 describes the curves of constant rms voltage. The rms of the voltage fluctuations e' given by the hot-wire anemometer and made dimensionless by the mean value are adjusted for a nearly equal sensitivity to mass flow and stagnation temperature fluctuations. One can see that the rms of e' decreases under the effect of expansion in the inner layer, strongly increases in the mixing layer, reaches a maximum in

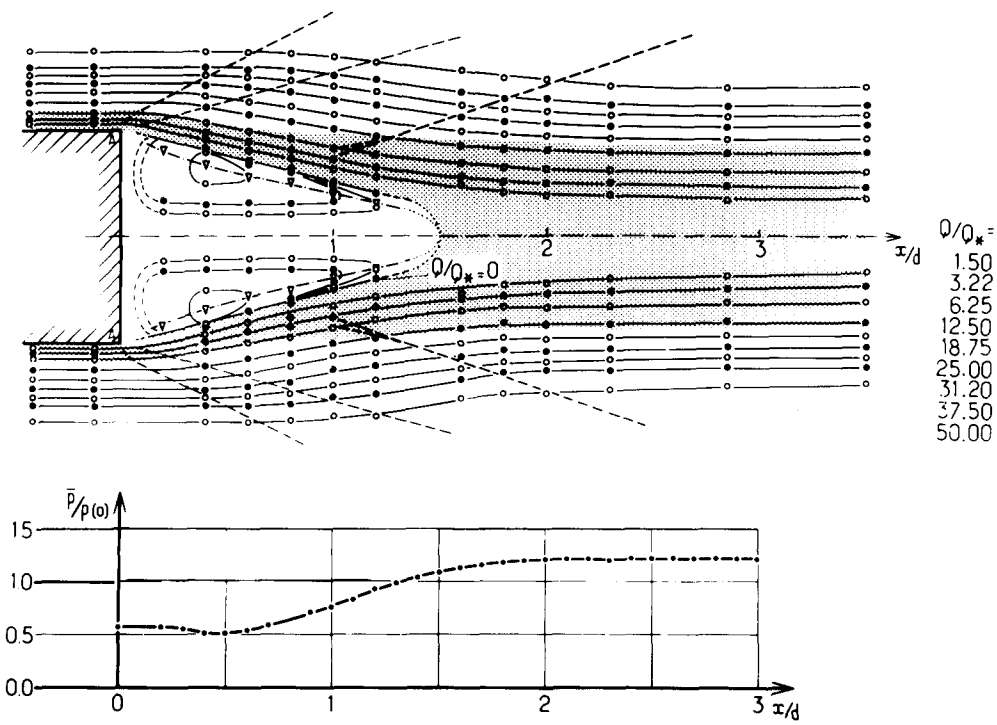

FIG. 13. Near turbulent wake of a cylinder supersonic flow at $M = 2.3$. The mass-weighted average streamlines are shown above and the mean pressure in the mixing layer is given below.

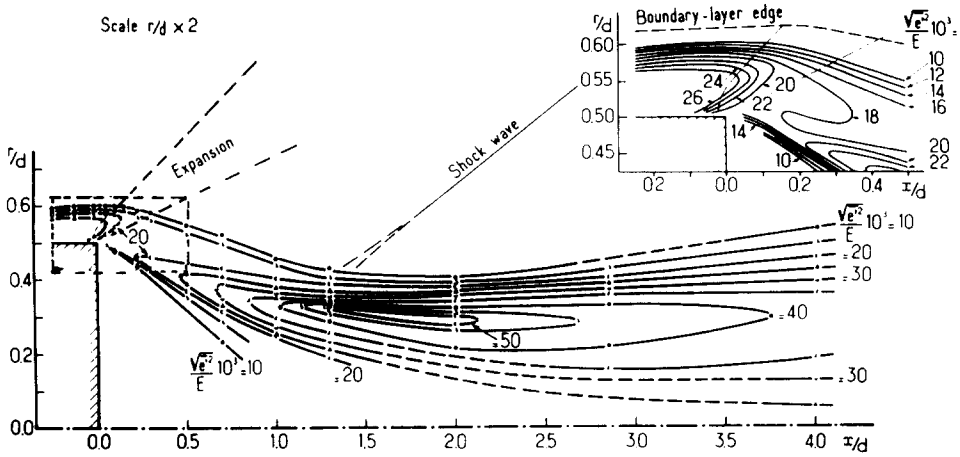

FIG. 14. Curves of constant dimensionless standard deviation of turbulent fluctuations in the near wake of a cylinder at $M = 2.3$.

the core at a distance between 1.3 and 2 diameters downstream of the cylinder, and then slowly decreases. The velocity–temperature correlation coefficient does not differ much from the usual value -0.8 found in self-preserving flows as discussed later.

The measurement of the turbulent velocity production has been made for the longitudinal fluctuation component but are not complete. The results tend to show, according to the analytical considerations, that the isovolumetric production is often positive as in subsonic flows and the enthalpic production and dilation are either positive or negative. In a strongly negative pressure gradient, for example, in an expansion fan with acceleration, the isovolumetric production is enhanced by the negative enthalpic and dilation terms, and the production is negative. In the present case, the pressure gradient in the near wake is positive and isovolumetric production is dominant with the enthalpic and compression production being weakly positive.

C. Interaction of a boundary layer with an expansion fan

To clarify with a better accuracy, the behavior of turbulence in supersonic flows strongly out of equilibrium, the interactions of a boundary layer with an expansion fan and shock were investigated. The explored boundary layer developed on a plane wall, encountered a deflection of 12°, and expanded without separation. The nominal Mach number was 1.76 and the Reynolds number based on the momentum thickness was about 5000.[49,50,53] Figure 15 shows the model with the mass-weighted average streamlines and the mean pressure distribution at the wall where the mean mass flux is defined as $Q^* \equiv (1/\delta) \int_0^\delta \bar{\rho}\tilde{u}/\rho a) dy$.

Figure 16 gives the evolution of the variance of the longitudinal fluctuations $\overline{u_1'^2}$ normalized with the free stream velocity upstream. The arrows show the correspondence, for each mean streamline, between the intensity in the boundary layer upstream and downstream of the expansion fan. One can see the strong decrease of turbulence $\overline{u_1'^2}$, mainly in the inner part of the boundary layer. The effect of dissipation, evaluated with the assumption that it is equal to the production upstream, is weak. The primary decrease of the variance is due to the density and pressure variations as in the expansion region of the axisymmetrical near wake.

An analytical calculation has been made[52] based on the Reynolds stresses equations written with mass-weighted averages[24,58] and using the assumptions of rapid distortion, the strong Reynolds analogy relation, conservation of velocity–temperature correlation (Sec. IID) and modeling the pressure–velocity correlations. This permits the separate evaluation of the effects of the different terms of the equations and illustrates the importance of the density and pressure gradients. The computations are consistent with the

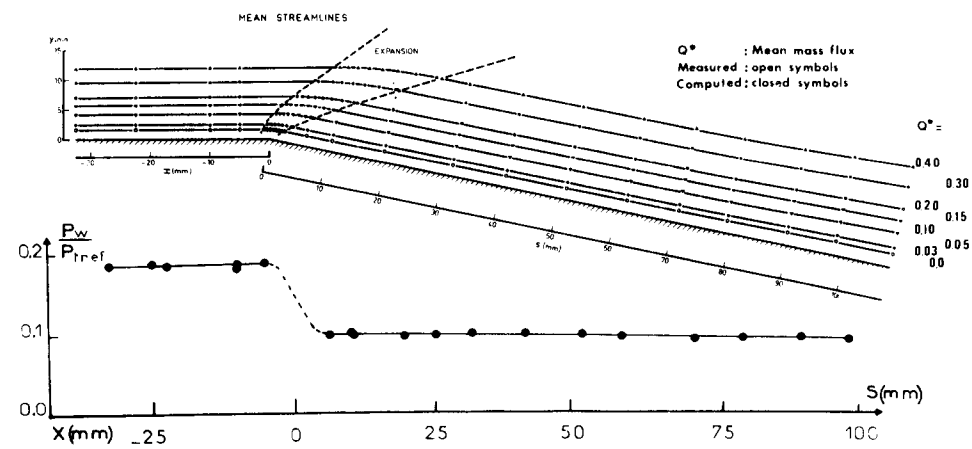

FIG. 15. Turbulent supersonic boundary layer with an expansion fan at $M = 1.76$. The mass-weighted average streamlines are shown above and the mean pressure at the wall is given below.

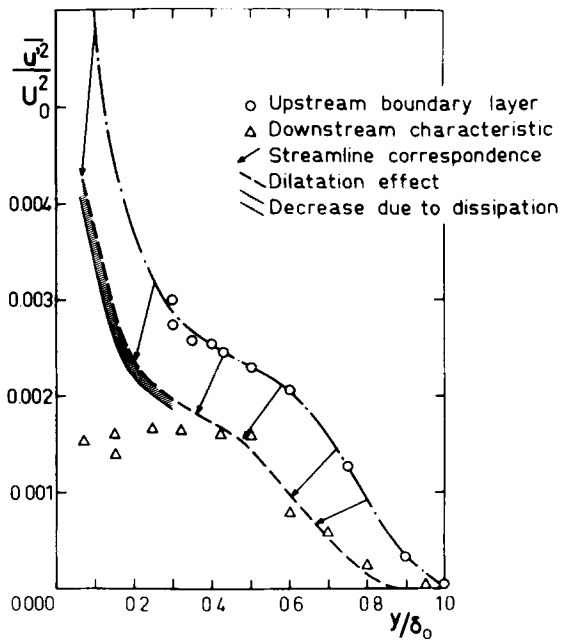

FIG. 16. Evolution of the velocity variance through an expansion fan in a turbulent supersonic boundary layer with $M = 1.76$.

measured decrease of $\overline{u_1'^2}$ which is approximately 60% of its original value upstream. Correspondingly the analysis indicates the other Reynolds stress components, such as $\overline{u_2'^2}$, $\overline{u_3'^2}$, and $\overline{u_1'u_2'}$ will decrease, respectively, to 50%, 80%, and 30% of their values before the expansion.

D. Interaction of the boundary layer with a shock wave

The boundary layer investigated developed on a flat plate and encountered a 6° turning angle which produced a shock-induced compression with no separation. The nominal Mach number was 2.3 and the Reynolds number based on momentum thickness was 4200.[50,51,52] Figure 17 shows the model and the mean pressure distribution at the wall. Figure 18 gives the longitudinal velocity intensity of turbulence upstream and downstream of the compression

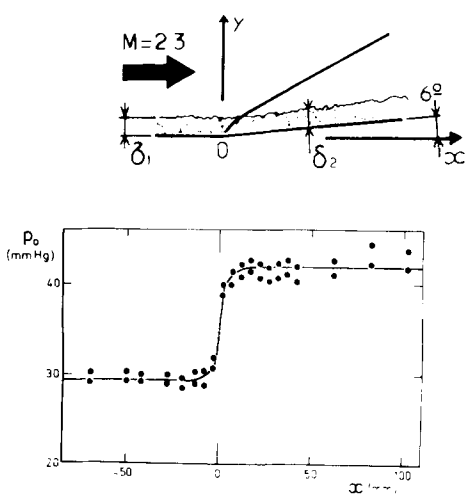

FIG. 17. Sketch of a turbulent supersonic boundary layer with a shock wave. The mean pressure at the wall at $M = 2.3$ is shown below.

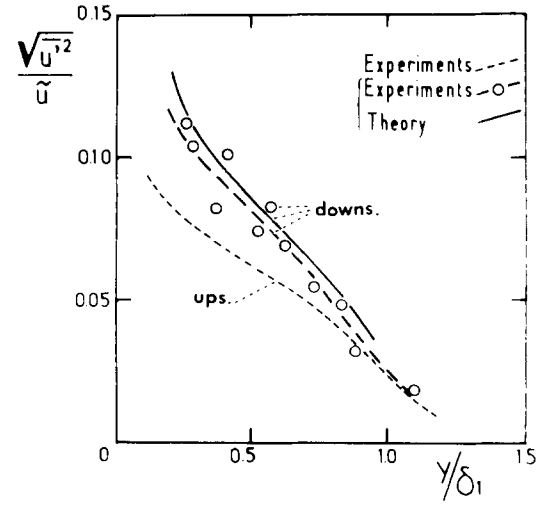

FIG. 18. Evolution of the velocity fluctuations through a shock wave in a turbulent supersonic boundary layer with $M = 2.3$.

zone. The level of turbulence increased in the boundary layer. Analogous results were obtained for the temperature fluctuations.

An analysis was performed using the equations with mass-weighted averages for Reynolds stresses,[58,59] an assumption of rapid distortion, and a Lagrangian type transformation with a model having a discontinuity in the shock-wave zone.[51,52] The computed values of the longitudinal velocity fluctuations variance are consistent with the data. In addition, the theory gives some indications of the evolution of the other components of the Reynolds stresses which are not yet measured. The largest increase of velocity variance is found in the direction normal to the shock wave.

E. Strong Reynolds analogy and the velocity–temperature coefficient of correlation. Common properties of the three types of flows

The strong Reynolds analogy relationship for the three types of investigated nonequilibrium supersonic flows has been calculated and appears[48–53,60] in Fig. 19. Although the

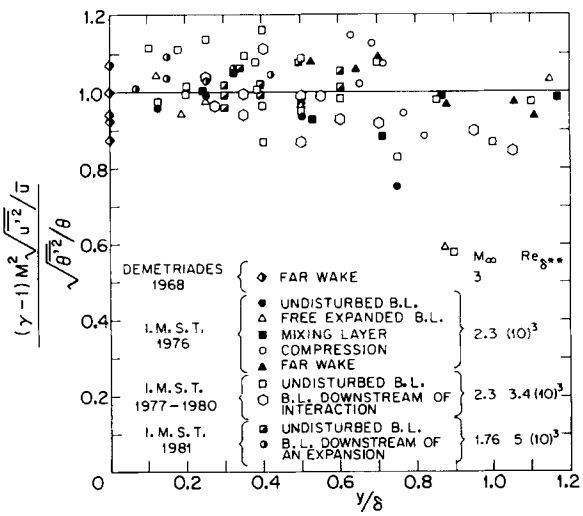

FIG. 19. Strong Reynolds analogy relation for various supersonic flows.

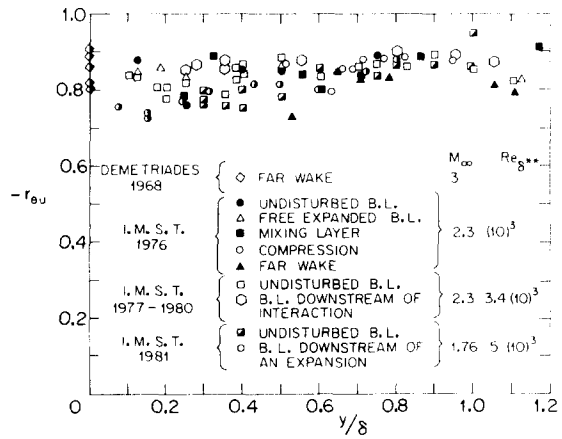

FIG. 20. Coefficient of velocity–temperature correlation for various supersonic flows.

analytical demonstration by Young[61] of the strong Reynolds analogy,

$$(\overline{\theta'^2})^{1/2}/\bar{\theta} \simeq (\gamma - 1)M^2(\overline{u_1'^2})^{1/2}(\tilde{u}_1)^{-1}, \tag{11}$$

requires there be no mean–pressure gradient, the experiments discussed earlier and others show that this relation applies in all three types of flows investigated in which there are strong pressure gradients (Fig. 19).

The velocity–temperature correlation coefficients for these nonequilibrium flows are plotted in Fig. 20.[48–53,60] These coefficients of approximately -0.8 agree with the usual values found in supersonic boundary layers in equilibrium.

F. Conclusion

In equilibrium supersonic flows, the turbulence does not differ much from that of a subsonic flow with heat sources. In the present cases of strongly nonequilibrium supersonic flows, one must also account for the effects of density fluctuations interacting with pressure gradients, i.e., the decrease of turbulence in expansion and increase in compression, as shown by measurements (Secs. IIB, IIC, and IID) and explained by analytical considerations (Sec. IIA).

ACKNOWLEDGMENTS

The author wishes to thank Dr. R. F. Blackwelder who revised this manuscript.

These investigations have been supported mainly by the Office National d'Etudes et Recherches Aérospatiales, Centre National de la Recherche Scientifique (C. N. R. S.), the U. S. Air Force Office of Scientific Research and N. A. T. O.

[1]A. Favre, Ministère Production Industrielle, Brevet Invention GR 12-CL 3, No. 924800, Paris (1946). U. S. Patent No. 2, 693, 908 (26 August 1947).

[2]A. Favre, presented at the Sixth International Congress of Applied Mechanics, Paris University, 1946 (unpublished); also see Refs. 3 and 4.

[3]A. Favre, in *Proceedings of the 1948 Seventh International Congress of Applied Mechanics,* London, edited by H. Levy (Her Majesty's Stationery Office, London, 1949), Vol. 2, pp. 44–55.

[4]A. Favre, Office National Etudes et Recherches Aéronautiques, Paris, Publication No. 67, pp. 1–65 1953.

[5]A. Favre, presented at the Second All Union Congress of Theoretical and Applied Mechanics, Moscow, 1964.

[6]MEXAHUKA, 2•90 (Moscow, 1965, pp. 70–99, in Russian); A. Favre, J. Appl. Mech., Ser. E, **32**, 2 (1965), p. 261.

[7]A. Favre, J. Gaviglio, and R. Dumas, in *Proceedings of the 1952 Eighth International Congress of Applied Mechanics,* Istambul, edited by Karim Erim (Edition Technique de la Faculté des Sciences, Istambul, 1953), pp. 307–314; La Recherche Aéronautique, Paris, Publication No. 31, (1953) pp. 37–44; in English: NACA T. M. 1371, Washington, 1955.

[8]A. Favre, J. Gaviglio, and R. Dumas, in *Proceedings of the 1952 Eight International Congress of Applied Mechanics,* Istambul, edited by Karim Erim (Edition Technique de la Faculté des Sciences, Istambul, 1953, pp. 314–324; La Recherche Aéronautique, Paris No. 32, 1953, pp. 21–28; in English: NACA T. M. 1370, Washington, 1955.

[9]A. Favre, J. Gaviglio, and R. Dumas, Recherche Aéronaut. Paris, No. 38 1954, pp. 7–12; No. 39, 1954, pp. 27–29; No. 40, pp. 7–14 1954.

[10]A. Favre, J. Gaviglio, and R. Dumas, in *Proceedings of the 1956 Ninth International Congress of Applied Mechanics,* Brussels (Brussels University, 1957), Vol. 4, pp. 213–233.

[11]A. Favre, J. Gaviglio, and R. Dumas, J. Fluid Mech. **2**, part 4, 313 (1957).

[12]A. Favre, J. Gaviglio, and R. Dumas, J. Fluid Mech. **3**, part 4, 344 (1958).

[13]A. Favre, J. Gaviglio, and R. Dumas, Office National d'Etudes et Recherches Aéronautiques, Publication No. 92, Paris, 1958, pp. 1–107.

[14]A. Favre, J. Gaviglio, and R. Dumas, in *Proceedings of the 1961 Colloque International No. 108 du Centre National de la Recherche Scientifique, Mécanique de la Turbulence,* Marseille, edited by A. Favre (C. N. R. S., Paris, 1962), pp. 419–445; English translation: *The Mechanics of Turbulence* (Gordon and Breach, New York, 1964), pp. 419–445.

[15]A. Favre, J. Gaviglio, and R. Dumas, in *Proceedings of the 1966 IUGG–IUTAM Symposium on Boundary Layers and Turbulence,* Kyoto, edited by K. F. Bowden, F. Frenkiel, and I. Tani [Phys. Fluids **10**, 138 (Sept., Part II, 1967)].

[16]A. Favre, J. Gaviglio, and J. Fohr, in *Proceedings of the 1964 Eleventh International Congress of Applied Mechanics,* Munich, edited by H. Görtler (Springer, Berlin, 1964), pp. 878–888.

[17]A. Favre, J. Gaviglio, and E. Verollet, in *Proceedings of the 1968 Twelfth International Congress of Applied Mechanics,* Stanford University, edited by M. Hetényi, and W. G. Vincenti (Springer, New York, 1969), pp. 192–208.

[18]R. Dumas, E. Arzoumanian, and A. Favre, in *Proceedings of the 1972 Thirteenth International Congress for Theoretical and Applied Mechanics,* Moscow (unpublished); also see Ref. 19.

[19]R. Dumas, E. Arzoumanian, and A. Favre, C. R. Acad. Sci. Paris, Ser. A **277**, 759 (1973).

[20]L. Fulachier, J. Giovanangeli, R. Dumas, L. Kovasznay, and A. Favre, C. R. Acad. Sci., Ser. B **278**, 683 (1974).

[21]L. Fulachier, J. Giovanangeli, R. Dumas, L. Kovasznay, and A. Favre, C. R. Acad. Sci., Paris, Ser. B **278**, 999 (1974).

[22]R. Dumas, E. Arzoumanian, and A. Favre (unpublished); I. M. S. T., Report, Marseille (1974).

[23]R. Dumas, L. Fulachier, E. Arzoumanian, and A. Favre, J. Phys. (Paris) Colloq. C. 1, Supp. No. 1, **37**, C1-181 (1976).

[24]A. Favre, L. Kovasznay, R. Dumas, J. Gaviglio, and M. Coantic, *La turbulence en mécanique des fluides: bases théoriques et expérimentales, méthodes statistiques* (Gauthier-Villars, Paris,1976), Part II, pp. 24–75.

[25]R. Dumas, L. Fulachier, E. Arzoumanian, L. Kovasznay, and A. Favre, in *Abstracts of the 1976 Fourteenth International Congress of Theoretical and Applied Mechanics,* Delft, edited by W. T. Koiter (North Holland, Amsterdam, 1976), 504 (also see Refs. 20, 21, and 23).

[26]L. Fulachier, E. Arzoumanian, and R. Dumas, in *Structure and Mechanics of Turbulence II,* edited by H. H. Fernholz, E. Krause (Springer, Berlin, 1978), pp. 188–198.

[27]R. Dumas, E. Arzoumanian, and L. Fulachier, C. R. Acad. Sci. Paris Ser. B **284**, p. 487 (1977).

[28]M. Elena, L. Fulachier, and R. Dumas, AGARD Conference Proceedings No. 271, 1979, pp. 2-1 to 2-21.

[29]L. Kovasznay and A. Favre, I. M. S. T., Report (1978), pp. 10, 11 and pp. 50, 51.

[30]E. Arzoumanian, R. Dumas, and A. Favre, C. R. Acad. Sci., Paris, Ser. B **286**, 113 (1978).

[31]R. Dumas, E. Arzoumanian, L. Fulachier, and A. Favre, Arch. Mech. **30**, 421 (1978).

[32]M. Coantic, A. Ramamonjiarisoa, P. Mestayer, F. Resch, and A. Favre, J. Geophys. Res. **86**, 6607 (1981).

[33]G. I. Taylor, Proc. R. Soc. London Ser. A **164**, 476 (1938).

[34]J. Hinze, *Turbulence* (McGraw-Hill, New York, 1975).

[35]G. Comte-Bellot and S. Corrsin, J. Fluid Mech. **48**, 273 (1971).

[36]L. Kovasznay, V. Kibens, and R. Blackwelder, J. Fluid Mech. **41**, 283

(1970).
[37]J. Sabot and G. Comte-Bellot, C. R. Acad. Sci. Ser. A-**274**, 1647 (1972).
[38]F. H. Champagne, V. G. Harris, and S. Corrsin, J. Fluid Mech. **41**, 81 (1970).
[39]I. Wygnanski and H. Fiedler, J. Fluid Mech. **38**, 577 (1960).
[40]I. Wygnanski and H. Fiedler, J. Fluid Mech. **41**, 327 (1970).
[41]J. Bonnet and T. Alziary de Roquefort, in *Proceedings of the 1980 Symposium ICHMT-IUTAM, Structures of Turbulence and Heat and Mass Transfer,* Dubrovnik, edited by Z. Zaric (McGraw-Hill, New York, pp. 297–316).
[42]S. Corrsin, J. Atmos. Sci. **20**, 115 (1963).
[43]L. Fulachier, Thése Doct. Sci., I. M. S. T., Marseille, 1972.
[44]S. J. Kline, W. C. Reynolds, F. A. Schraub, and P. W. Runstadler, J. Fluid Mech. **30**, 741 (1967).
[45]D. Schlien and S. Corrsin, J. Heat Mass Transfer **19**, 285 (1976).
[46]L. S. G. Kovasznay, J. Aero. Sci. **20**, 657 (1953).
[47]J. P. Dussauge, J. Gaviglio, and A. Favre, C. R. Acad. Sci., Paris Ser., B 953 (1974).
[48]J. Gaviglio, J. P. Dussauge, J. F. Debieve, and A. Favre, C. R. Acad. Sci., Paris, Ser. B, **282**, 445 (1976).
[49]J. Gaviglio, J. P. Dussauge, J. F. Debieve, and A. Favre, Phys. Fluids **20**, Part II, S179-S192, (1977).
[50]A. Favre, in *Proceedings of the 1980 AFOSR-HTTM Stanford Conference on Complex Turbulent Flows*, edited by S. J. Kline, B. J. Cantwell, and G. M. Lilley (Stanford University, Stanford, CA, 1981), Vol. I, pp. 482–483.
[51]J. F. Debieve, H. Gouin, and J. Gaviglio, in *Proceedings of the 1980 Symposium ICHMT-IUTAM, Structures of Turbulence and Heat and Mass Transfer*, Dubrovnik, edited by Z. Zaric (McGraw-Hill, New York, 1982), pp. 277–297.
[52]J. F. Debieve, C. R. Acad. Sci., Paris, Ser. B **291**, p. 133 (1980).
[53]J. P. Dussauge, Thése Doc. és-Sc., I. M. S. T., Marseille, 1981).
[54]A. Favre, C. R. Acad. Sci., Paris, Ser. A **246**, 2576 (1958); **246**, 2723 (1958); **246**, 2839 (1958); **246**, 3216 (1958).
[55]A. Favre, J. Mécanique **4**, 361 (1965); **4**, 391 (1965).
[56]A. Favre, *U. S. S. R. Acad. Sci. 60th Birthday, L. I. Sedov* (Nauka, Moscow, 1969) pp. 483–511; English tranls.: *Problems of Hydrodynamics and Continuum Mechanics* (Society for Industrial and Applied Mathematics, Philadelphia, PA, 1969), pp. 231–266.
[57]A. Favre, in *Proceedings of the 1971 Symposia Mathematica Caculo delle Probabilita*, edited by Istituto Nazionale di Alta Matematica (Academic, New York, 1972), pp. 371–390.
[58]A. Favre, in *Proceedings of the 1975 Fifth Canadian Congress of Applied Mechanics*, Fredericton, edited by G. Dhatt, Jaeger, and A. Cardou (University of New Brunswick, New Brunswick, 1975), G. 3.
[59]A. Favre, in *Proceedings of the 1978 Dynamic Flow Conference. Dynamic Measurements in Unsteady Flows*, edited by L. S. Kovasznay, A. Favre, P. Buchave, and L. Fulachier, I. M. S. T., Marseille, 1978; Johns Hopkins University, Baltimore, 1978 (Technical Editor B. W. Hansen, DISA Elektronic A/S, DK-2740 Skovlunde, Denmark), pp. 617–627.
[60]A. Demetriades, J. Fluid Mech. **34**, 465 (1968).
[61]A. D. Young, College of Aeronautics, Cranfield, Report No. 42 (1951).